Wave-vector-dependent electron-phonon coupling and the charge-density-wave transition in $TbTe_3$

M. Maschek,[1] S. Rosenkranz,[2] R. Heid,[1] A. H. Said,[3] P. Giraldo-Gallo,[4,6] I. R. Fisher,[5,6] and F. Weber[1]

[1]*Karlsruhe Institute of Technology, Institute of Solid State Physics, 76021 Karlsruhe, Germany*

[2]*Materials Science Division, Argonne National Laboratory, Argonne, Illinois 60439, USA*

[3]*Advanced Photon Source, Argonne National Laboratory, Argonne, Illinois 60439, USA*

[4]*Geballe Laboratory for Advanced Physics and Department of Physics, Stanford University, Stanford, California 94305, USA*

[5]*Geballe Laboratory for Advanced Physics and Department of Applied Physics, Stanford University, Stanford, California 94305, USA*

[6]*The Stanford Institute for Materials and Energy Sciences, SLAC National Accelerator Laboratory, Menlo Park, California 94025, USA*

(Received 5 November 2014; revised manuscript received 10 June 2015; published 29 June 2015)

We present a high-energy-resolution inelastic x-ray scattering investigation of the soft phonon mode in the charge-density-wave (CDW) system $TbTe_3$. We analyze our data based on lattice dynamical calculations using density-functional-perturbation theory and find clear evidence that strongly momentum-dependent electron-phonon coupling defines the periodicity of the CDW superstructure: Our experiment reveals strong phonon softening and increased phonon linewidths over a large part in reciprocal space adjacent to the CDW ordering vector $\boldsymbol{q}_{\mathrm{CDW}} = (0,0,0.3)$. Further, $\boldsymbol{q}_{\mathrm{CDW}}$ is clearly offset from the wave vector of (weak) Fermi surface nesting $\boldsymbol{q}_{\mathrm{FS}} = (0,0,0.25)$, and our detailed analysis indicates that electron-phonon coupling is responsible for this shift. Hence, we can add $TbTe_3$, which was previously considered as a canonical CDW compound following the Peierls scenario, to the list of distinct charge-density-wave materials characterized by momentum-dependent electron-phonon coupling.

DOI: 10.1103/PhysRevB.91.235146 PACS number(s): 78.70.Ck, 63.20.dd, 71.15.Mb, 71.45.Lr

The concept of a charge-density wave (CDW) leads back to the seminal work of Peierls [1], in which he demonstrated that a one-dimensional metallic chain of atoms is unstable towards a phase transition in the presence of finite electron-phonon coupling (EPC). This phase is characterized by an oscillating electronic charge density, i.e., a CDW, and a periodic lattice distortion having the same periodicity. The corresponding ordering wave vector is of pure electronic origin and reflects the perfect nesting of the one-dimensional system at $\boldsymbol{q}_{\mathrm{CDW}} = 2\boldsymbol{k}_F$. Since then, CDW ordered phases, also in two-dimensional materials, are commonly associated with a nesting geometry of the electronic structure. In recent years, however, it has become evident that CDW order without nesting, a possibility derived theoretically by Chan and Heine in 1973 [2], does occur in canonical CDW materials such as $2H$-$NbSe_2$ [3–5]. Without nesting, the periodicity of the superstructure is then defined by the momentum dependence of EPC.

The rare-earth tritellurides $R\mathrm{Te}_3$ (R = La, Ce, Gd, Tb, ...) are prime examples of CDW ordered ground states. Angle-resolved photoemission spectroscopy (ARPES) measurements [6,7] of several rare-earth tritelluride compounds including $TbTe_3$ lead to the assumption of a nesting driven CDW order and, hence, $R\mathrm{Te}_3$ are often used as canonical Peierls-like CDW systems. On the other hand, theoretical investigations in rare-earth tritellurides [4] revealed a nesting feature, i.e., a peak in the imaginary part of the electronic susceptibility $\chi''(\boldsymbol{q})$ at a wave vector different from the observed CDW ordering wave vector. Nonetheless, the real and imaginary parts of $\chi(\boldsymbol{q})$ in those calculations show a broad enhancement in the correct direction but the wave vector was still not correctly predicted [$\boldsymbol{q}_{\mathrm{FS}} = (0, 0, 0.25)$ compared to the observed ordering wave vector $\boldsymbol{q}_{\mathrm{CDW}} = (0, 0, 0.295)$] [8]. More importantly, as the authors pointed out, this modest enhancement was far from a divergence and as such was likely insufficient to drive the CDW instability. A recent theoretical analysis of Raman spectroscopy measurements [9] in $ErTe_3$ further corroborates that the weak nesting geometry is not identical to the ordering wave vector and enhanced electron-phonon coupling might be important.

We use high energy-resolution inelastic x-ray scattering (IXS) to investigate the lattice dynamical properties at the CDW phase transition in $TbTe_3$. We combine our experimental results with detailed lattice dynamical calculations and demonstrate that the difference between $\boldsymbol{q}_{\mathrm{CDW}}$ and $\boldsymbol{q}_{\mathrm{FS}}$ originates from strongly momentum-dependent EPC in the case of $TbTe_3$, and likely also in other $R\mathrm{Te}_3$.

The experiment was performed at the XOR 30-ID (HERIX) beamline [10,11] of the Advanced Photon Source, Argonne National Laboratory. The sample was a high-quality single crystal, grown by slow cooling a self-flux with a CDW transition at $T_{\mathrm{CDW}} = 330\,\mathrm{K}$ [12] and dimensions of $1\times1\times0.1\ \mathrm{mm}^3$. The components (Q_h, Q_k, Q_l) of the scattering vector are expressed in reciprocal lattice units (r.l.u.) $[Q_h, Q_k, Q_l = (h^*2\pi/a, k^*2\pi/b, l^*2\pi/c)$ with the lattice constants $a = 4.316\,\text{Å}$, $b = 25.5\,\text{Å}$, and $c = 4.31\,\text{Å}$ of the orthorhombic unit cell]. Phonon excitations in constant-$\boldsymbol{Q}$ scans were fitted with damped harmonic oscillator functions [13]. We extracted the intrinsic phonon linewidth Γ of the damped harmonic oscillator (DHO) function by convoluting our fit with the experimental resolution of 1.5 meV. Thus, we obtain phonon energies $\omega_q = \sqrt{\tilde{\omega}_q^2 - \Gamma^2}$, where $\tilde{\omega}_q$ is the phonon energy renormalized only by the real part of the susceptibility χ and Γ is closely related to the imaginary part of $T_{\mathrm{CDW}}\,\chi$ (see the discussion below).

Figure 1 shows IXS data taken well above and at the CDW transition temperature. Along the [001] direction we find two phonon branches with high intensities at $\boldsymbol{Q} = (3, 1, l)$, $0.1 \leqslant l \leqslant 0.5$: An optic branch disperses from 15 to 12 meV in the measured wave-vector range. Near halfway towards the zone boundary we observe strong scattering intensities also below 10 meV, with the maximum scattering rate located at a dip

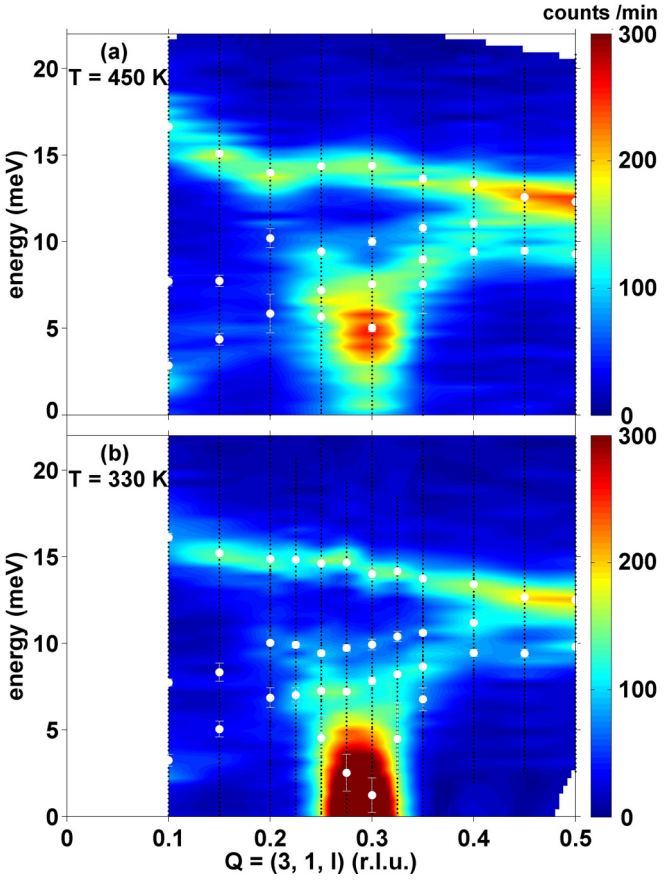

FIG. 1. (Color online) Measured intensities of transverse phonons along the [001] direction at (a) $T = 450$ K and (b) $T = T_{CDW} = 330$ K. Vertical dotted lines represent the actually performed constant-$\boldsymbol{Q}$ scans at $\boldsymbol{Q} = (3, 1, l)$, $0.1 \leqslant l \leqslant 0.5$, summarized in color-coded contour maps. White dots are fitted phonon energies.

in the phonon dispersion at $l = 0.3$ at $T = 450$ K [Fig. 1(a)]. The latter phonon is indeed the soft phonon mode, which is renormalized close to zero energy at T_{CDW} [Fig. 1(b)], whereas the optic mode is not much affected by the temperature change. Figure 2 summarizes constant-$\boldsymbol{Q}$ scans at $l = 0.3$, i.e., within the experimental resolution of the CDW ordering wave vector $\boldsymbol{q}_{CDW} = (0, 0, 0.295)$ [8], at various temperatures $320\ \text{K} \leqslant T \leqslant 450$ K. At high temperatures [Figs. 2(a) and 2(b)] we see that there are two additional weak phonon modes at intermediate energies, $E = 7.5$ and 10 meV. However, they are barely visible close to on top of the huge intensity of the soft mode, and we will therefore limit our discussion to the two phonon modes dominating the spectra. The lowest-energy mode at $T = 450$ K softens gradually from around 5 meV [Fig. 2(a)] to nearly zero (within the experimental error bar) at $T_{CDW} = 330$ K [Fig. 2(c)]. Here, the elastic scattering of the CDW superstructure peak emerges and dominates the spectrum at 320 K [Fig. 2(d)].

Figure 3 summarizes the measured dispersion at T_{CDW} [Fig. 3(a)], the observed temperature dependence of the energies [Fig. 3(b)], and the linewidths Γ [Fig. 3(c)] of the soft mode and the optic mode at $\boldsymbol{q}_{CDW}$. The soft phonon mode dispersion is clearly visible with a dip around $\boldsymbol{q}_{CDW}$ and the extracted temperature dependences show the expected

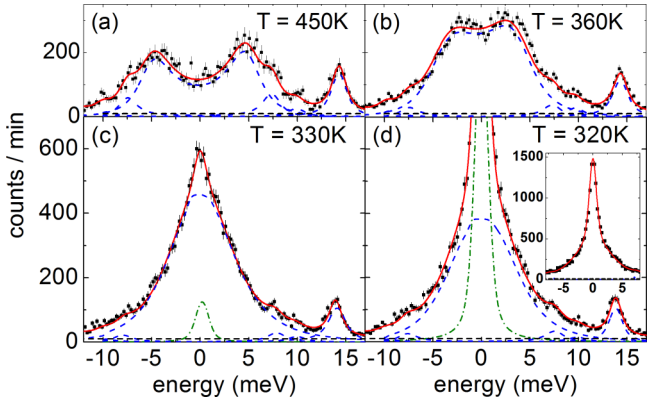

FIG. 2. (Color online) Energy scans taken at $\boldsymbol{Q} = (3,1,0.3)$ and $320\ \text{K} \leqslant T \leqslant 450$ K. Solid (red) lines are fits consisting of damped harmonic oscillators (inelastic, blue dashed lines) and a pseudo-Voigt function (elastic, green dashed-dotted lines). The horizontal dashed black line is the estimated experimental background. The inset in (d) shows the full intensity range at zero energy of the scan at $T = 320$ K.

softening [Fig. 3(b)] and broadening [Fig. 3(c)] strongest at T_{CDW}. For comparison, we show the corresponding, practically temperature-independent, values for the optic mode at $\boldsymbol{q}_{CDW}$.

For a more detailed analysis we performed *ab initio* calculations for the lattice dynamical properties based on density-functional-perturbation theory (DFPT) using the high-temperature orthorhombic structure present at $T > T_{CDW}$. In $TbTe_3$, the f states of Tb are localized and shifted away from the Fermi energy. Therefore, they are expected to play no role

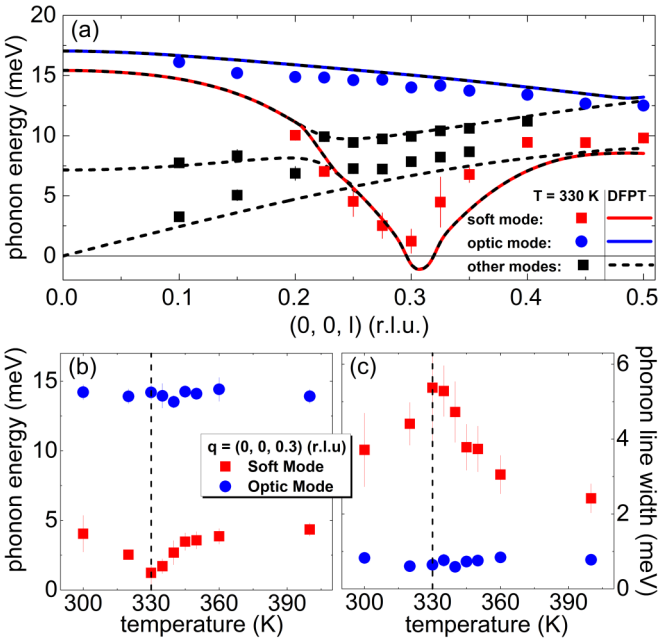

FIG. 3. (Color online) (a) Comparison between calculated (dashed lines) and observed ($T = 330$ K) energies of transverse phonon modes along the [001] direction (squares). Red and blue lines mark the dispersion of the soft phonon mode character and a strong optic mode, respectively. The temperature dependences of the phonon energy and linewidth of the marked modes at $\boldsymbol{q} = (0,0,0.3)$ are shown in (b) and (c), respectively. The dashed line denotes the transition temperature $T_{CDW} = 330$ K.

for the physics of the CDW [7,14]. To avoid complications with the f states in standard density-functional theory, we have performed our calculations for $LaTe_3$ in the framework of the mixed basis pseudopotential method [15]. Norm-conserving pseudopotentials were constructed following the scheme of Vanderbilt including $5s$ and $5p$ semicore states of La in the valence space but explicitly excluding $4f$ states [16]. The basis set consisted of plane waves up to 20 Ry complemented with local functions of s, p, and d symmetry at the La sites. For the exchange-correlation functional, the local-density approximation (LDA) was applied [17]. DFPT as implemented in the mixed basis pseudopotential method [18] was used to calculate phonon frequencies and electron-phonon coupling. An orthorhombic $24\times8\times24$ **k**-point mesh was employed in the phonon calculation, whereas an even denser $48\times12\times48$ mesh was used in the calculation of phonon linewidths to ensure proper convergence. This was combined with a standard smearing technique using a Gaussian broadening of 0.24 eV.

The calculated dispersion is in good agreement with our data at T_{CDW} [Fig. 3(a)], i.e., DFPT predicts the structural instability at the correct wave-vector position. Hence, we confirm that $4f$ states are not relevant for CDW formation in $TbTe_3$, in agreement with previous reports [4,7]. The calculated intensities for the phonon modes at $\boldsymbol{Q} = (3,1,l)$, $0.1 \leqslant l \leqslant 0.5$, are in excellent agreement with our IXS data, demonstrating that the predicted transverse optic mode is indeed the CDW soft mode. Hence, we can use DFPT to follow the character of the soft mode along the [001] wave-vector direction. We find that the soft mode at $\boldsymbol{q}_{CDW}$ in fact has an optic character. It starts out at the zone center at 15 meV (with zero spectral weight in the measured Brillouin zone) and slowly bends downward and exhibits two anticrossings with lower-energy branches of the same symmetry in short order just above and below an energy of $E = 5$ meV. Beyond $\boldsymbol{q}_{CDW}$ it disperses upwards again. In the following we refer to the described dispersion as the soft mode dispersion [marked red in Fig. 3(a)]. The dispersion of the high-energy optic branch is marked in blue and also shows good agreement with experiment.

In the standard theory of CDW order outlined by Chan and Heine [2], the properties of the soft phonon mode are directly connected to the electronic structure via the real and imaginary parts of the electronic susceptibility, $\chi'(\boldsymbol{q})$ and $\chi''(\boldsymbol{q})$. Whereas $\chi'(\boldsymbol{q})$ is mostly reflected in the renormalization of the phonon energy, $\chi''(\boldsymbol{q})$ is in first order proportional to the linewidth of the soft mode, which reflects the reduced lifetime due to EPC. The difference between the minimum in the calculated soft mode dispersion [Fig. 3(a), indicated by $\boldsymbol{q}_{SM}$ in Fig. 4(a)] and the maxima of both $\chi'(\boldsymbol{q})$ and $\chi''(\boldsymbol{q})$ [Fig. 4(a), $\chi'(\boldsymbol{q})$ and $\chi''(\boldsymbol{q})$ reproduced from Ref. [4]], which are clearly separated, is striking. According to Ref. [2], the strength of the phonon renormalization is proportional to the product $\chi(\boldsymbol{q}) \cdot \eta_{\boldsymbol{q}}^2$, which includes the squared averaged EPC matrix element $\eta_{\boldsymbol{q}}^2$. Thus, we assign the observed difference to a strongly momentum-dependent $\eta_{\boldsymbol{q}}^2$.

From our own calculations, we can extract the electronic joint density of states (EJDOS), which is directly related to $\chi''(\boldsymbol{q})$ and reflects the number of electronic states at the Fermi surface connected by a particular wave vector, i.e., the tendency to Fermi surface nesting. We find good

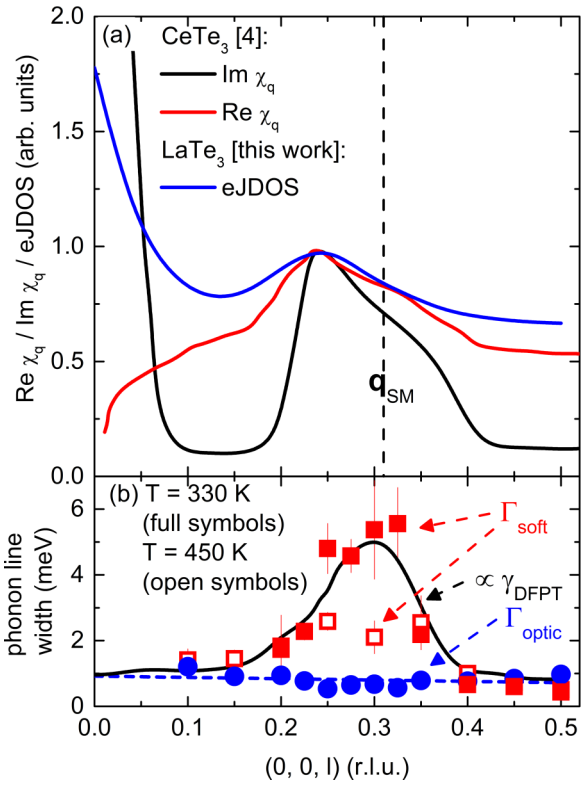

FIG. 4. (Color online) (a) Comparison of calculated real and imaginary part of the noninteracting electronic susceptibility χ_q for $CeTe_3$ extracted from Ref. [8] with the electronic joint density of states from DFPT in this work. The vertical dashed line indicates the position of the soft mode in the DFPT calculation. (b) Wave-vector dependences of linewidths of the soft mode Γ_{soft} (red squares) and optical mode Γ_{optic} (blue dots) at $T_{CDW} = 330$ K. Open symbols denote the values of Γ_{soft} at $T = 450$ K. The solid line represents a DFPT calculation of the linewidth of the soft mode. For comparison, it has an offset (dashed blue line) and is scaled (see text).

agreement of the wave-vector position of the maxima of the EJDOS and $\chi''(\boldsymbol{q})$ from Ref. [4] [Fig. 4(a)]. Based on this, we can calculate the electronic contribution to the phonon linewidth γ [Fig. 4(b)]. We again find an offset, now between the wave-vector positions of the maximum of γ and the EJDOS, where the former agrees well with the minimum of the soft mode dispersion [indicated by $\boldsymbol{q}_{SM}$ in Fig. 4(a)]. Hence, the momentum dependence of γ is set by $\eta_{\boldsymbol{q}}^2$ and the number of available electronic decay channels, i.e., the EJDOS [19]. Thus, the presence of a strongly momentum-dependent EPC matrix element $\eta_{\boldsymbol{q}}^2$ is demonstrated within our *ab initio* calculation.

Experimentally, the wave-vector range with large phonon linewidths Γ agrees well with the prediction of DFPT [Fig. 4(b)], corroborating our interpretation. Quantitatively, DFPT underestimates Γ by a factor of about 20. Indeed, we found in several studies that DFPT underestimates the experimental linewidths for soft phonon modes in the CDW compounds $NbSe_2$ [5,20] and $TiSe_2$ [21] but also in the superconductor YNi_2B_2C [22]. However, DFPT predictions were typically only a factor of 2 below the observed values in these compounds, and were assigned to anharmonic

contributions disregarded in DFPT. The much larger discrepancy for $TbTe_3$ originates in a much smaller calculated γ, whereas the experimental values of Γ in $TbTe_3$ and $NbSe_2$ [5] and also $TiSe_2$ [21] are comparable. Although it seems that the CDW in the rare-earth tritellurides is mainly related to Te states at the Fermi level, we cannot exclude that inclusion of $4f$ states into our calculations is required for an improved quantitative description. This cannot be tackled easily and is subject of future research.

Here, we argue that the obvious mismatch between maxima in $\chi(\boldsymbol{q})$ on the one side and the wave-vector position of the soft mode and the largest linewidth at $\boldsymbol{q}_{\mathrm{CDW}}$ on the other side, in particular, within the DFPT theory itself, demonstrates the defining influence of momentum-dependent EPC in $TbTe_3$. A similar proposal has been made based on Raman measurements in $ErTe_3$ [9]. Hence, a $\boldsymbol{q}$-dependent EPC is likely relevant for the whole family of rare-earth tritellurides, which is also supported by the fact that we can model the behavior of $TbTe_3$ rather well without taking into account $4f$ electrons. So far, the importance of momentum-dependent EPC was shown for compounds, for which the nesting scenario was questioned already for a long time [5,23]. Our results for $TbTe_3$ demonstrate that EPC needs to be investigated even if the periodicity of the CDW order is "roughly" explained by the electronic structure.

In conclusion, we reported inelastic x-ray measurements and DFPT calculations of the soft phonon mode on entering the CDW ordered phase in $TbTe_3$. Our observation of a broad softening and enhanced phonon linewidths over a large range of wave vectors is well explained by DFPT lattice dynamical calculations. A more detailed analysis shows that the wave-vector dependency of EPC in $TbTe_3$ is defining the ordering wave vector $\boldsymbol{q}_{\mathrm{CDW}}$ in contrast to the standard Fermi surface nesting scenario.

M.M. and F.W. were supported by the Helmholtz Society under Contract No. VH-NG-840. Work at Argonne was supported by the U.S. Department of Energy, Office of Science, Office of Basic Energy Sciences, under Contract No. DE-AC02-06CH11357. The work at Stanford University was supported by the DOE, Office of Basic Energy Science, under Contract No. DE-AC02-76SF00515.

[1] R. E. Peierls, *Quantum Theory of Solids* (Oxford University Press, New York, 1955).
[2] S. K. Chan and V. Heine, J. Phys. F **3**, 795 (1973).
[3] M. D. Johannes, I. I. Mazin, and C. A. Howells, Phys. Rev. B **73**, 205102 (2006).
[4] M. D. Johannes and I. I. Mazin, Phys. Rev. B **77**, 165135 (2008).
[5] F. Weber, S. Rosenkranz, J. P. Castellan, R. Osborn, R. Hott, R. Heid, K. P. Bohnen, T. Egami, A. H. Said, and D. Reznik, Phys. Rev. Lett. **107**, 107403 (2011).
[6] J. Laverock, S. B. Dugdale, Z. Major, M. A. Alam, N. Ru, I. R. Fisher, G. Santi, and E. Bruno, Phys. Rev. B **71**, 085114 (2005).
[7] V. Brouet, W. L. Yang, X. J. Zhou, Z. Hussain, R. G. Moore, R. He, D. H. Lu, Z. X. Shen, J. Laverock, S. B. Dugdale, N. Ru, and I. R. Fisher, Phys. Rev. B **77**, 235104 (2008).
[8] N. Ru, J. H. Chu, and I. R. Fisher, Phys. Rev. B **78**, 012410 (2008).
[9] H.-M. Eiter, M. Lavagnini, R. Hackl, E. A. Nowadnick, A. F. Kemper, T. P. Devereaux, J.-H. Chu, J. G. Analytis, I. R. Fisher, and L. Degiorgi, Proc. Natl. Acad. Sci. USA **110**, 64 (2013).
[10] A. H. Said, H. Sinn, and R. Divan, J. Synchrotron Radiat. **18**, 492 (2011).
[11] T. S. Toellner, A. Alatas, and A. H. Said, J. Synchrotron Radiat. **18**, 605 (2011).
[12] N. Ru and I. R. Fisher, Phys. Rev. B **73**, 033101 (2006).
[13] B. Fåk and B. Dorner, Physica B **234–236**, 1107 (1997).
[14] V. Brouet, W. L. Yang, X. J. Zhou, Z. Hussain, N. Ru, K. Y. Shin, I. R. Fisher, and Z. X. Shen, Phys. Rev. Lett. **93**, 126405 (2004).
[15] B. Meyer and M. Fähnle (Max-Planck-Institut für Metallforschung, Stuttgart).
[16] D. Vanderbilt, Phys. Rev. B **32**, 8412 (1985).
[17] L. Hedin and B. I. Lundqvis, J Phys. C: Solid State Phys. **4**, 2064 (1971).
[18] R. Heid and K. P. Bohnen, Phys. Rev. B **60**, R3709 (1999).
[19] R. Heid, K.-P. Bohnen, and B. Renker, in *Advances in Solid State Physics*, edited by B. Kramer (Springer, Berlin, 2002), Vol. 42, p. 293.
[20] F. Weber, R. Hott, R. Heid, K. P. Bohnen, S. Rosenkranz, J. P. Castellan, R. Osborn, A. H. Said, B. M. Leu, and D. Reznik, Phys. Rev. B **87**, 245111 (2013).
[21] F. Weber, S. Rosenkranz, J. P. Castellan, R. Osborn, G. Karapetrov, R. Hott, R. Heid, K. P. Bohnen, and A. Alatas, Phys. Rev. Lett. **107**, 266401 (2011).
[22] F. Weber, L. Pintschovius, W. Reichardt, R. Heid, K. P. Bohnen, A. Kreyssig, D. Reznik, and K. Hradil, Phys. Rev. B **89**, 104503 (2014).
[23] M. Leroux, M. Le Tacon, M. Calandra, L. Cario, M.-A. Méasson, P. Diener, E. Borrissenko, A. Bosak, and P. Rodière, Phys. Rev. B **86**, 155125 (2012).